Spontaneous Formation of Microwrinkles on Metal Microdot Arrays by Shrinkage of Thermal Shrinkable Substrate

Hiroshi Yabu,*,†,‡ Yasutaka Matsuo,#,‡,§ Kuniharu Ijiro,#,‡,§ Fumiaki Nishino,|| Toshihiko Takaki,|| Masahiro Kuwahara,|| and Masatsugu Shimomura*,†,‡,⊥

Institute of Multidisciplinary Research for Advanced Materials (IMRAM), Tohoku University, 2-1-1 Katahira, Aoba-Ku, Sendai, 980-8577 Japan, Core Research for Evolutional Science and Technology (CREST), Japan Science and Technology Agency (JST), 5 Sanbancho, Chiyoda-Ku, Tokyo, 102-00752 Japan, Research Institute for Electronic Science (RIES), Hokkaido University, N21W10 Kita-Ku, Sapporo, 001-0021 Japan, Material Science Laboratory, Mitsui Chemical Inc., Nagaura, Sodegaura, Chiba, 299-0265 Japan, and WPI-Advanced Institute for Materials Research (AIMR), Tohoku University, 2-1-1 Katahira, Aoba-Ku, Sendai, 980-8577 Japan

ABSTRACT Honeycomb-patterned polymer films prepared by the simple casting of a polymer solution under humid conditions were used as templates for metal microdot arrays formed on shrinkable polymer substrates by metal sputtering. After thermal shrinkage of the substrate, the periodicity of the metal microdots was reduced. In addition, microwrinkles were formed on the metal microdots. The wavelength and arrangement of the microwrinkles were changed with the metal sputtering time and the diameter of the metal microdots. A clear confinement effect was observed in the formation of the microwrinkles.

KEYWORDS: self-organization • metal microdot • confinement • microwrinkles • shrinkable substrate

1. INTRODUCTION

Honeycomb-patterned polymer films (1) prepared by the simple casting of polymer solutions under humid conditions are attractive materials based on their potential applications as separation membranes (2), photonic crystals (3), cell culturing substrates (4), and so on (5). Water droplets condense on the cooled surface of the polymer solution because of evaporation cooling, and they are then packed by capillary force (6). After evaporation of the solvent, the traces of water droplets remain in the polymer film as regularly arrayed micro pores. This breath figure (7) method can be used for the patterning of a wide variety of materials, including engineering plastics (8), conductive polymers (9), biodegradable polymers (10), and metallic compounds (11).

The honeycomb-patterned polymer film has a double-layered structure. Two porous layers are connected by many thin pillars located at the corners of small hexagons, reflecting the structure of the close-packed template water droplets. Secondary physical and chemical processing of honeycomb-patterned polymer films provides a wide variety of novel micro- and nanostructured polymer films. For example, a single-layered honeycomb-patterned film can be formed by thermal melting of the pillars when the original double-layered structure is annealed at temperatures above the glass transition temperature, T_g. (12) A pincushion structure is prepared by simply peeling off the top-layer with adhesive tape (13), such pincushion-structured films exhibit superhydrophobic properties (14). In addition, micro lens arrays and physical copies of honeycomb-patterned films can be prepared by molding and replication of the honeycomb-patterned films (15).

Recently, metal−polymer hybrid nanostructures, based on the honeycomb-patterned polymer films, and their unique properties have been reported. Silver-plated honeycomb- and pincushion-structured films were fabricated by electroless plating of Ag onto Pt/Pd layers sputtered on the films (16). Metal dome and polymer pincushion hybrid structures can also be prepared by electroless plating and peeling off the top layer of the honeycomb-patterned polymer film (17). These surfaces exhibit superhydrophobic properties with strong adhesion of water droplets. The pores of a honeycomb-patterned film can be used as templates for other metal−polymer hybrid surface patterns. Hadziioannou et al. reported that hexagonally arranged Al dots were formed on a glass substrate by vapor-deposition of Althrough the pores of a template honeycomb-patterned polymer film, followed by washing of the template (18a). We also have reported that dots of Au and Pt/Pd alloy can be formed on silicon, glass, or polymer film substrates after discharge sputtering of the metals and subsequent washing of the template honeycomb-patterned polymer films (18b). Electroless deposition of Ag on Pt/Pd dots provides Ag dots (18c). These metal−polymer

* Corresponding author. E-mail: yabu@tagen.tohoku.ac.jp.
Received for review June 14, 2009 and accepted December 14, 2009
† IMRAM, Tohoku University.
‡ Japan Science and Technology Agency.
# Core Research for Evolutional Science and Technology.
§ Hokkaido University.
|| Mitsui Chemical Inc.
⊥ AIMR, Tohoku University.
DOI: 10.1021/am900768e

Chart 1

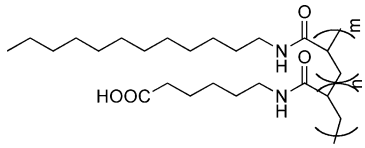

hybrid structures can be applied as porous electrodes, photonic crystals, and metamaterials.

Thermal shrinkable polymer film, which is a stretched polymer substrate, shrinks when it is heated at over T_g. (19) Surface patterns formed on a shrinkable polymer film can also be shrunk after heat treatment (20). Recently, we reported the shrinkage of a poly(butadiene) honeycomb-patterned film on a stretched polymer film by heat treatment, which resulted in miniaturization of the periodicity of the pores (21).

In this paper, we report the formation of metal dot arrays on a shrinkable polymer substrate by the sputtering of metals though the honeycomb pores and subsequent thermal shrinking. The surface topologies of metal dot arrays before and after shrinking are discussed.

4. EXPERIMENTAL SECTION

Preparation of Honeycomb-Patterned Films. Polystyrene (PS, M_w = 280 000, Aldrich, USA) and amphiphilic copolymer **1** (Chart 1) (22) were dissolved in chloroform to prepare a 5 mg/mL solution. The solution (1−7.5 mL)was cast onto a 9 cm diameter Petri dish, and then humidified air (20 °C, relative humidity 60−80%) was applied vertically to the solution surface at a rate of 4 L/min. After complete evaporation of solvent and condensed water, the surface structure of the film was observed using an optical microscope (BH-2, Olympus, Japan), and detailed structure was observed using scanning electron microscopy (SEM; S-3500N, Hitachi, Japan).

Transfer of the Periodic Structures onto the Stretched Polymer Films. Before transfer of the film, UV-ozone treatment was performed to reduce the mechanical strength of the honeycomb-patterned PS film (Figure 1). The honeycomb-patterned PS film was then peeled from the substrate in water and the floating film was placed upside down on a shrinkable polymer substrate (1.5 times 2 biaxial-stretched APEL8008T, Mitsui Chemical Company, Inc., Japan). After being dried in vacuo, the film was pressed with a polydimethylsiloxane (PDMS) elastomer (Sylgard 184, Dow Corning, USA) to break the pillars supporting the double layer structure of the honeycomb-patterned film. The single layer of honeycomb-patterned PS film adhered to the PDMS elastomer was peeled away with removal of the PDMS. The other layer of honeycomb-patterned PS film remained on the shrinkable polymer substrate. Pt and Pd were sputtered for 20−80 s using a discharge ion sputtering apparatus (discharge current ca. 20 mV, E-1030 Hitachi, Japan). After sputtering, the template film was removed using a sheet of adhesive tape (Scotch Tape, 3M, USA).

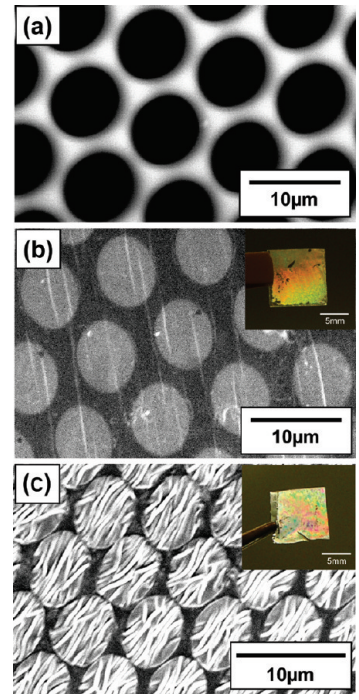

FIGURE 2. Photograph and SEM images of (a) honeycomb-patterned PS film, (b) metal dots formed on the thermal shrinkable substrate before, and (c) after heating.

Shrinkage of the Films. The pattern-transferred film was annealed on a hot stage (Rinkam600, Japan Hi-tech, Japan) at 100 °C for 1 min. After annealing, the surface structure was observed using SEM. The SEM images were analyzed using image processing software (Image SXM, NIH, USA).

3. RESULTS AND DISCUSSION

A typical SEM image of the microporous template film is shown in Figure 2a. The pores of the film are of uniform size and are arranged hexagonally. After sputtering Pt/Pd, the

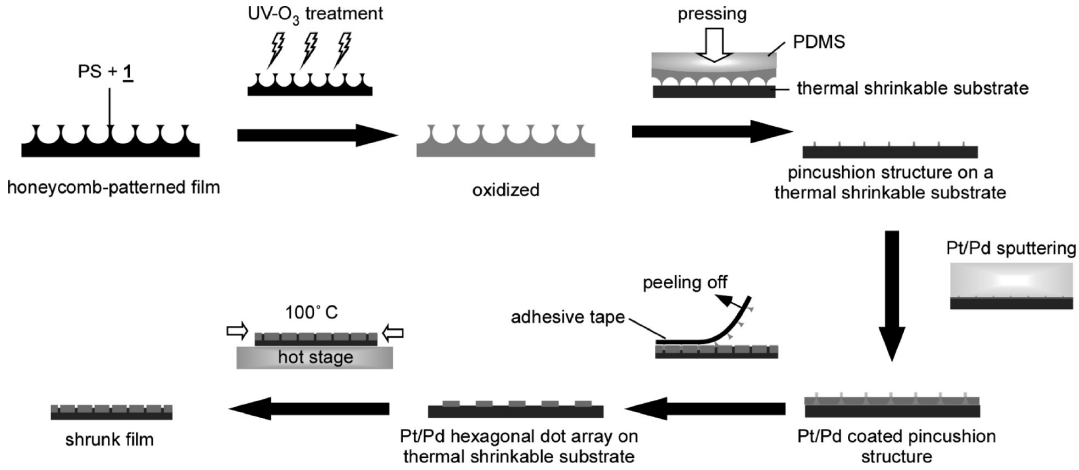

FIGURE 1. Schematic illustration of metal dot preparation onto the stretched polymer film and its thermal contraction.

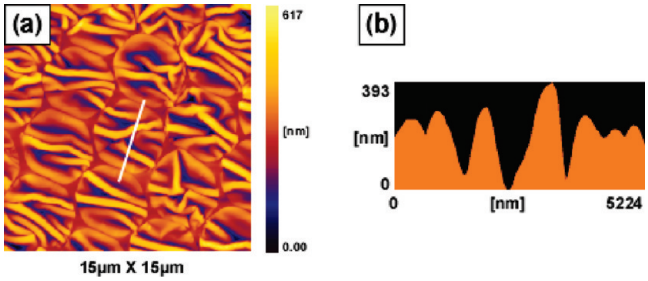

FIGURE 3. (a) Topographic AFM image and (b) a cross-section of microwrinkles on metal microdot structure. The cross-sectional image in b was obtained on the white line on a.

template top layer was removed by a sheet of adhesive tape. A photograph of the microdots prepared on the thermal shrinkable substrate is shown in the inset of Figure 2b. The interference color of the film indicates that a highly periodic metal structure was formed on the surface of the film. The transferred dot structure shows a clear hexagonally arranged microdot structure (Figure 2b). The average center-to-center distance and diameter of the microdots in this case is ca. 8.0 and 5.0 μm, respectively.

After heating, the size of the film was reduced by shrinkage. An SEM image of the surface structure of the shrunk film is shown in Figure 2c, and a photograph of the shrunk film is shown in the inset of Figure 2c. The center-to-center distance between the dots was shrunk to 6.5 μm; however, the microdot size was reduced by only 0.2 μm after film shrinkage. The film shrinkage was mainly caused by shrinkage of the space between the dots. In addition, wrinkles were formed on the surface of the dots. The substrate was shrunk by heat treatment; however, the metal microdots did not follow the shrinkage of the substrate. As a result, buckling (23) occurred and microwrinkles were formed on the surface of the metal microdots.

Figure 3a shows a typical atomic force microscopy (AFM) image of the metal microdot arrays that clearly shows the microwrinkles formed on metal microdots after shrinkage. The height of the microwrinkles was estimated to be ca. 400 nm from the cross-section of the AFM image (Figure 3b).

To reveal the effect of sputtering time, which is proportional to the thickness of the metal layer, on microwrinkle formation, we changed the sputtering time from 20 to 80 s. Figure 4 shows SEM images of the hexagonally arranged metal microdots that were sputtered for different times and formed on the stretched polymer film after shrinkage. In each case, the center-to-center distances of the metal microdots were shrunk by thermal contraction of the film. On the other hand, the width of the microwrinkles and the spacing between microwrinkles increased when the sputtering time increased. Irregular and narrow (ca. 200 nm) microwrinkles were formed after shrinkage on the metal dots formed by sputtering for 20 s. The wrinkles formed on metal microdots produced by sputtering for 40 s were arranged unidirectionally and the width of the microwrinkles increased. This tendency is same in the case of metal dots formed by sputtering for 60 and 80 s.

Metal microdots were formed on shrinkable polymer films that were stretched 1.5 times on each two-dimensional

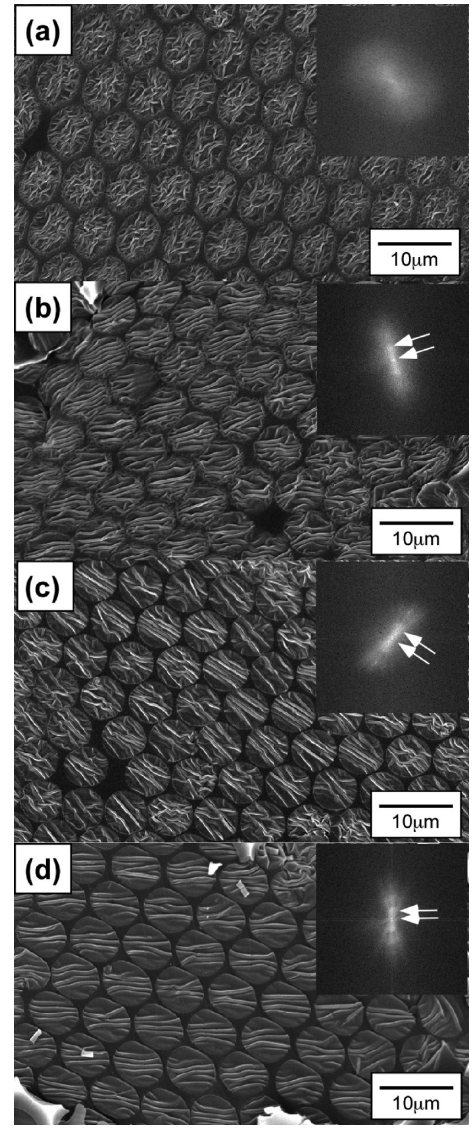

FIGURE 4. SEM images of metal dots of different sputtering time formed on the stretched polymer film after thermal contraction ((a) 20, (b) 40, (c) 60, and (d) 80 s, respectively). Each inset image is the FFT of 25 μm $\times$ 25 μm of the SEM image.

(2D) axis. It is known that microwrinkles are formed on various hard materials that are surface coated on elastic polymer films; the critical wavelength of such microwrinkles (λ) is expressed by (24)

$$\lambda = 2\lambda h[(1 - \nu_s^2)E_t/(3(1 - \nu_t^2)E_s)]^{1/3} \quad (1)$$

where h is the thickness of the top layer, ν_s and ν_f are the Poisson ratios of the substrate and top layers, respectively. E_s and E_t are the Young's moduli of the substrate and top layers, respectively. The substrate and top layers in this case are APEL8008T and platinum; therefore, ν_s (25), ν_t, E_s, E_t are -0.34, -0.377, 2.4 GPa, 16.8 GPa, respectively. The thickness of the platinum layer is calculated as 10, 21, 43, and 85 nm for sputtering times of 20, 40, 60, and 80 s, respectively. When these values are substituted as h, the resulting critical wavelengths λ are 150, 315, 645, and 1 275 nm, respectively. Figure 5 shows the theoretically calculated

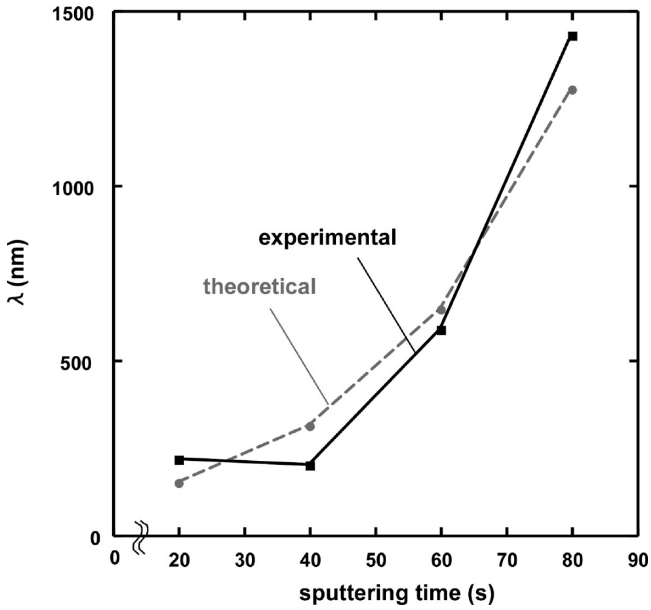

FIGURE 5. Plot of experimental and theoretical wavelengths of wrinkles as a function of sputtering time.

values of the critical wavelengths and the experimentally observed wavelengths of the microwrinkles, as measured from SEM images of the films. The theoretical and real values are in good agreement, which indicates that the wavelength of the microwrinkles on the metal dots are dominated primarily by the mechanical properties of the top and substrate layers of the structures.

2D fast Fourier transformation (FFT) of the SEM images (inset images in Figure 5) indicate that the orientation of the microwrinkles becomes aligned with increasing thickness of the metal layer. The FFT image of the 20 s sputtered sample shows indistinct spots, whereas clearer spots are observed in the FFT images of the 40−80 s-sputtered samples. The distance between peaks decreased with increasing sputtering time. These results indicate that the wrinkle wavelengths increase and become well-aligned with increasing sputtering time.

There are two reasons for the alignment of microwrinkles; one is the anisotropy of the shrinkable polymer substrate and the other is the confinement effect of the microdot. The shrinkable substrate used in this study is a biaxial-stretched polymer film, which is basically prepared by stretching the polymer film in one direction after the other. The polymer molecules in the film are perpendicularly reoriented at the second stretching, thus, the film has hysteretic shrinkage that depends on the stretching order, and the hysteresis may affect the orientation of wrinkles. The lateral confinement of the metal microdot structure also affects the orientation of microwrinkles. Crosby et al. reported that well-organized microwrinkles were formed on a surface oxidized polydimethylsiloxane microlens, depending on the oxidation time and size of microlens (26). The microwrinkles were well-aligned with increasing oxidation time (equivalent to an increase in the thickness of the "hard" layer) and decreasing size of the microlens. Finally, the wrinkles disappeared when the lens size became smaller

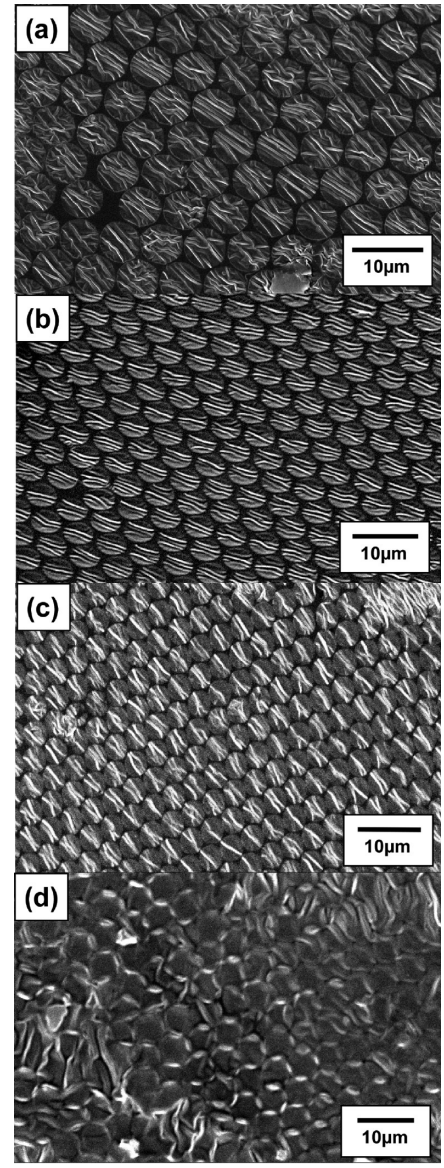

FIGURE 6. SEM images of metal dots of different diameters formed on the stretched polymer film after thermal contraction: (a) 7.0, (b) 5.7, (c)4.1, and (d) 2.6 μm, respectively.

than the wavelength of the microwrinkles. The same confinement effect was also observed in this study.

Figure 6 shows the effect of metal dot size on the microwrinkles in metal microdot array films with microdot diameters of (a) 7.0, (b) 5.7, (c) 4.1, and (d) 2.6 μm that were prepared by sputtering for 60 s. The metal dots maintain their circular structure after shrinkage, as shown in Figure 5. It is noteworthy that the number of wrinkles decreased when the size of the microdots decreased. In Figure 6a, the average number of microwrinkles is 5, but this is decreased to 3 and 2 in images b and c, respectively, in Figure 6, and finally, the microwrinkles disappear when the size of the metal microdot becomes smaller than 2 μm (Figure 6d).

Therefore, the effect of size on the microwrinkle formation of metal microdots is confirmed. Whitesides et al. reported that lower stress is applied to the region near the edge of a microdot (24). Thus, the edge of the metal microdots did not form wrinkles. Furthermore, in the case

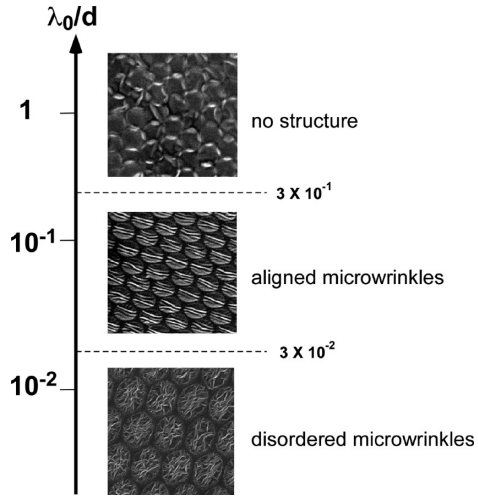

FIGURE 7. Relation between the value of λ_0/d and surface structure of the metal microdots.

of 2 μm diameter metal microdots, the edge effect dominates over the entire individual microdot, and as a result, lower stress is applied to the metal microdots.

These results indicate that the controlling factor of microwrinkle formation is the ratio between the wavelength of the microwrinkles and the diameter of the microdot. Figure 7 shows the relation between λ_0/d and the surface structure of a shrunken metal microdot array (λ_0 is the wavelength of the microwrinkle calculated from the thickness of the metal layer, and d is a diameter of the metal microdot). When the value of λ_0/d was smaller than 3.0×10^{-2}, the microwrinkles had a disordered structure. However, well-aligned microwrinkles were formed on the metal microdots when the value of λ_0/d was in the range from 3×10^{-2} to 3×10^{-1}. When the value of λ_0/d was larger than 3×10^{-1}, no wrinkles were formed. These results also support a lateral confinement effect of the size of metal microdot on microwrinkle structure.

4. CONCLUSION

The preparation of metal microdot structures on stretched polymer films was demonstrated. After thermal contraction of the film, the center-to-center distances of the metal microdots were reduced. The metal microdots formed had periodic sub-micrometer-sized wrinkles. The formation of microwrinkles was affected by the thickness and diameter of the metal microdots and lateral confinement affects the formation of the microwrinkle structures.

REFERENCES AND NOTES

(1) (a) Widawski, G.; Rawiso, M.; François, B. *Nature* **1994**, *369*, 387. (b) Maruyama, N.; Koito, T.; Sawadaishi, T.; Karthaus, O.; Ijiro, K.; Nishi, N.; Tokura, S.; Nishimura, S.; Shimomura, M. *Supramol. Sci.* **1998**, *5*, 331. (c) Jenekhe, S. A.; Chen, X. L. *Science* **1999**, *283*, 372. (d) Stenzel-Rosenbaum, M. H.; Davis, T. P.; Fane, A. G.; Chen, V. *Angew. Chem., Int. Ed.* **2001**, *40* (18), 3428. (e) Srinivasarao, M.; Collings, D.; Philips, A.; Patel, S. *Science* **2001**, *292*, 79. (f) Shimomura, M., Dissipative Structures and Dynamic Processes for Mesoscopic Polymer Patterning. In *Nanocrystals Forming Mesoscopic Structures*; Pileni, M. P., Ed.; Wiley-VCH: Weinheim, Germany, 2005; pp 157–171.

(2) Tanaka, M.; Takebayashi, M.; Miyama, M.; Nishida, J.; Shimomura, M. *Biomed. Mater. Eng.* **2004**, *14* (4), 439.

(3) Kurono, N.; Shimada, R.; Ishihara, T.; Shimomura, M. *Mol. Cryst. Liq. Cryst.* **2002**, *377*, 285.

(4) Nishikawa, T.; Ookura, R.; Nishida, J.; Arai, K.; Hayashi, J.; Kurono, N.; Sawadaishi, T.; Hara, M.; Shimomura, M. *Langmuir* **2002**, *18* (15), 5734.

(5) (a) Gover, L. V.; Goldbach, M.; Bashmakov, I. A.; Butylina, I. B.; Parishi, J. *Phys. Rev. B* **2000**, *62* (3), 2201. (b) Yabu, H.; Shimomura, M. *Chem. Mater.* **2005**, *17* (21), 5231.

(6) Karthaus, O.; Maruyama, N.; Cieren, X.; Shimomura, M.; Hasegawa, H.; Hashimoto, T. *Langmuir* **2000**, *16* (15), 6071.

(7) Beysens, D. *Atomos. Res.* **1995**, *39*, 215.

(8) Yabu, H.; Tanaka, M.; Ijiro, K.; Shimomura, M. *Langmuir* **2003**, *19* (15), 6297.

(9) Song, L.; Bly, R. K.; Wilson, J. N.; Bakbak, S.; Park, J. O.; Srinibasarao, M.; Bunz, U. H. F. *Adv. Mater.* **2004**, *16* (2), 115.

(10) (a) Nishikawa, T.; Nishida, J.; Ookura, R.; Nishimura, S.; Wada, S.; Karino, T.; Shimomura, M. *Mater. Sci. Eng., C* **1999**, *8–9*, 495. (b) Yamamoto, S.; Tanaka, M.; Sunami, H.; Ito, E.; Yamashita, S.; Morita, Y.; Shimomura, M. *Langmuir* **2007**, *23* (15), 8114.

(11) (a) Karthaus, O.; Cieren, X.; Maruyama, N.; Shimomura, M. *Mater. Sci. Eng., C* **1999**, *10*, 103. (b) Yabu, H.; Shimomura, M. *Int. J. Nanosci.* **2002**, *1* (5–6), 673.

(12) Yabu, H.; S himomura, M. *Langmuir* **2006**, *22* (11), 4992.

(13) Yabu, H.; Takebayashi, M.; Tanaka, M.; Shimomura, M. *Langmuir* **2005**, *21* (8), 3235.

(14) Yabu, H.; Hirai, Y.; Kojima, M.; Shimomura, M. *J. Adhesion Sci. Technol.* **2008**, *7* (3), 856.

(15) Yabu, H.; Shimomura, M. *Langmuir* **2005**, *21* (5), 1709.

(16) Yabu, H.; Hirai, Y.; Shimomura, M. *Langmuir* **2006**, *22* (23), 9760.

(17) Ishii, D.; Yabu, H.; Shimomura, M. *Chem. Mater.* **2009**, *21* (9), 1799.

(18) (a) de Boer, B.; Stalmach, U.; Nijland, H.; Hadziioannou, G. *Adv. Mater.* **2000**, *12* (21), 1581. (b) Shimomura, M.; Koito, T.; Maruyama, N.; Arai, K.; Nishida, J.; Gråsjo, L.; Karthaus, O.; Ijiro, K. *Mol. Cryst. Liq. Cryst.* **1998**, *322*, 305. (c) Hirai, Y.; Yabu, H.; Shimomura, M. *Colloids Surf., A* **2008**, *313–314*, 312.

(19) Hirai, Y.; Yabu, H.; Shimomura, M. *Macromol. Symp.* **2008**, *267*, 95.

(20) Yabu, H.; Shimomura, M. *Polym. J.* **2008**, *40* (6)), 534.

(21) Yabu, H.; Matsuo, Y.; Ijiro, K.; Nishino, F.; Takaki, T.; Kuwahara, M.; Shimomura, M. *Adv. Mater.* **2008**, *20* (21), 4200.

(22) Nishida, J.; Nishikawa, K.; Nishimura, S.-I.; Wada, S.; Karino, T.; Nishikawa, T.; Ijiro, K.; Shimomura, M. *Polym. J.* **2002**, *34* (3), 166.

(23) (a) Pocivavsek, L.; Dellsy, R.; Kern, A.; Johnson, S.; Lin, B.; Lee, K. Y. C.; Cerda, E. *Science* **2008**, *320*, 912. (b) Khang, D.-Y.; Rogers, J. A.; Lee, H. H. *Adv. Funct. Mater.* **2008**, *18*, 1.

(24) Bowden, N.; Brittain, S.; Evans, A. G.; Hutchinson, J. W.; Whitesides, G. M. *Nature* **1998**, *14*, 148.

(25) The Piosson ratio of APEL8008T is not available from the Mitsui Chemicals Inc,, thus, we used the value of polystyrene, which is one of the representative polymer materials, in this experiment.

(26) Chan, E. P.; Crosby, A. J. *Adv. Mater.* **2006**, *18*, 3238.

AM900768E